1962

Asymmetric neutron flux distribution in the UTR-10 reactor.

Phillips, Alan Randolph.

Iowa State University of Science and Technology

ASYMMETRIC NEUTRON FLUX DISTRIBUTION IN THE UTR-10 REACTOR

by

Alan Randolph Phillips

A Thesis Submitted to the
Graduate Faculty in Partial Fulfillment of
The Requirements for the Degree of
MASTER OF SCIENCE

Major Subject: Nuclear Engineering

TABLE OF CONTENTS

INTRODUCTION

The UTR-10 reactor in operation at Iowa State University has been used to conduct training in reactor operation, for research in reactor physics and engineering, and to provide services in related fields where the requirements of the investigation are within the capabilities of the reactor. The experimental facilities of the reactor have been used in several projects reported in graduate student theses; however, none has involved an investigation of the neutron flux distribution within the core of the reactor.

The UTR-10, a heterogeneous, thermal reactor, has a core configuration of two fuel slabs separated by a graphite internal reflector. De-ionized light water acts as both moderator and coolant. The core is surrounded laterally by a graphite reflector, and the water in the aluminum core tanks provides an additional one foot thick reflector for both the top and bottom of the fuel slabs. Four moral rods, located adjacent to the core and inside the reflector, vary the reactivity. The two safety rods, located at the northwest and southeast corners as shown in Figure 1 (a), must be completely withdrawn when the reactor is in operation, and the shim-safety rod and the regulating rod, located at the northeast and southwest corners, respectively, control the reactor power level.

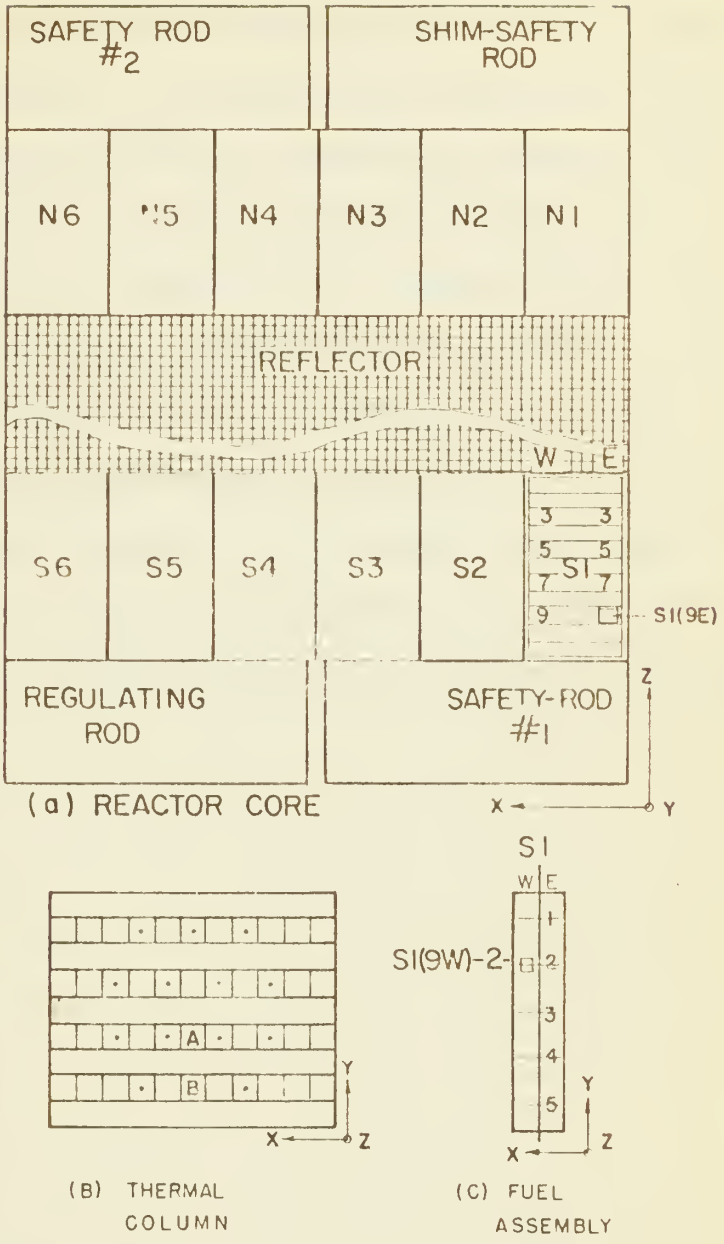

Figure 1. Station designations

The objective of this project was to examine the neutron flux distribution within the south core tank by determining the neutron activation of indium foils placed inside the fuel element assemblies. A limited flux survey was made in the north core tank to provide a basis for comparing the neutron flux distribution in the two sections of the core, and, in addition, a limited survey of the cadmium ratios in both sections was conducted to obtain an evaluation of the absolute thermal neutron flux at a few stations within the core. The investigation was conducted at a reactor power of 0.1 watt, and restrictions imposed on the control rods were that the regulating rod be completely withdrawn and that the shim-safety rod be manually controlled to regulate the reactor power level.

REVIEW OF LITERATURE

The core of the UTR-10 is divided into two fuel slabs separated by an 18 in. thick graphite internal reflector. Each slab contains six fuel elements, each of which consists of twelve fuel plates spaced at a nominal distance of 0.40 in. The fuel elements are supported in an aluminum tank which confines the flow of the light water moderator-coolant through the fuel assemblies. The limited space available in the core where a neutron detector may be located and the requirement for immersion of the detector in water while the reactor is in operation restrict the choice of neutron detector. The use of thin foils as neutron-activation detectors is compatible with these conditions, however. The foils offer certain distinct advantages, among which are:

(a) The small size permits their direct insertion into the core, and only a small correction is required to account for their disturbance of the flux.

(b) Immersion of the foils in the water inside the core presents no special difficulty.

(c) Flexibility in choice of stations to be observed within the core is permitted with the use of foils.

The ease with which the foils may be used to obtain a large number of observations throughout the core is advantageous. In comparison with foil detectors, some direct reading device

such as a miniature ion chamber would involve a more cumbersome installation within the core and increase the difficulty of determining the position of the detector within the core.

Neutron activation of gold and indium foils has been widely investigated as a means of determining the thermal neutron flux in a reactor. Price (11b) discusses the fundamental use of foil neutron detectors. The basic nuclear reaction of neutrons with indium is

$$49In^{115} + 0n^{1} \rightarrow 49In^{116} \rightarrow 50Sn^{116} + \beta$$

In^{116} exists in a metastable state and a ground state with respective half lives of 54.0 min. and 13 sec.; however, β decay of In^{116m} alone can be detected after waiting a few minutes for the short lived In^{116} to decay to an inconsequential level. Other reactions of fast neutrons with In^{115} may complicate the decay schemes, but the 54.0 min. period can be counted almost exclusively.

Activation of gold foil occurs as a result of the nuclear reaction

$$79Au^{197} + 0n^{1} \rightarrow 79Au^{198} \rightarrow 80Hg^{198} + \beta$$

Accompanying the β decay of Au^{198} is the emission of 0.41 Mev γ radiation. Cole (14) has preferred to use a γ radiation

detector in order to reduce the effects of foil self-absorption of γ radiation as compared with the absorption of β radiation. Klema and Ritchie (7) used the γ radiation from both indium and gold foils in their investigation of thermal neutron flux measurement in graphite.

During the period from 1955 to 1957 a study of absolute thermal neutron determination was made at North American Aviation, Inc., Downey, California. The report of this study gives an overall view of the basic problems. In Part I, Greenfield et al. (5) discuss using indium foil to measure cadmium ratios and the pertinent correction factors involved. Koontz et al. (8) report the effects of thickness on self-scattering, self-absorption, and backscattering of β particles from indium foil. Greenfield et al. (6) conclude the report with a discussion of determining absolute thermal neutron flux with the absolute specific disintegration rate of indium foils. The technique involved β particle counting in a windowless proportional counter with 2π geometry.

The correction of the observed activity induced in gold and indium foil has been the subject of many investigations. Both Skyrme (13) and Bothe (3) have developed theories for the effect of the neutron detector in a diffusion medium. Skyrme's theory was developed for a thin disc and included the effects of foil self-shielding and flux depression in the diffusion medium. Bothe's theory was developed for the flux

perturbation of spherical detectors, but Tittle (17) has modified the theoretical development and has shown experimentally that it can be applied to thin disc absorbers. Ritchie and Eldridge (12) present a theoretical discussion in extension of Bothe's and Skyrme's theories. Sola (14, p. 78) briefly reviews the findings of several other investigations and contributes his own data for gold foil in a graphite moderator. Kunstadter (9) presents corrections to be applied to the activity of neutron activated, cadmium-covered indium foils, and Martin (10) discusses these corrections for both gold and indium foils. For the most part, the investigations have confirmed Bothe's theory; however, Thompson (16), experimenting with indium foil in graphite, has obtained experimental results in closer agreement with Skyrme's theory than with Bothe's theory. Fitch and Drummond (4) have obtained experimental results for the neutron flux perturbation of indium foil in water, and their data support Bothe's theory. In a statement prefacing his review of the literature Sola (14, p. 78) remarks appropriately:

> A somewhat confusing impression arises from the different conclusions drawn by authors when they compare similar experiments with the existing theories. This is generally due to a lack of agreement on the definition of flux perturbation. Also, the different theories do not give the same results, presumably owing to differences in methods of approach.

LIST OF SYMBOLS

A	Foil activity, cpm./g.
A_s	Specific foil activity, saturated, cpm./g.
A_{se}	Saturation activity from epithermal neutrons, cpm./g.
A_{st}	Measured saturation activity from thermal neutrons, cpm./g.
A'_{st}	Saturation activity from thermal neutrons, corrected for flux depression, cpm./g.
$A_s(Cd)$	Total saturation activity of cadmium-covered foil, cpm./g.
CR	Cadmium ratio
d	Absorber average thickness, cm.
f_{Cd}	Cadmium correction factor
f_{th}	Flux perturbation factor
ln	Natural logarithm
N	Number of observed nuclear events, counts
R	Observed decay rate, cpm.
$\bar{R}$	Average decay rate of radionuclide, cpm.
R_0	Initial decay rate of foil at reactor shutdown, cpm.
r	Absorber radius, cm.
r_b	Background counting rate, cpm.
r_{obs}	Observed counting rate, cpm.
S_{cr}	Counting rate of standard source at time of counter

calibration, cpm.

S'_{cr} Counting rate of standard source at time of observation of foil, cpm.

T Foil irradiation time, min.

t Time, min.

$\bar{t}$ Time at which the average observed decay rate is applicable

t_1 Time at the beginning of observation

t_2 Time at the end of observation

W Foil weight, g.

α Probability that a neutron will be absorbed in a single traversal of a detector

Δ Time interval of observation, min.

δ Elapsed time after beginning of observation, min.

λ Radioactive decay constant, $min.^{-1}$

λ_{tr} Transport mean free path in moderator, cm.

ϕ_{th} Thermal neutron flux, $n/cm.^2$-sec.

Σ_a Macroscopic absorption cross section, $cm.^{-1}$

EXPERIMENTAL EQUIPMENT

Activation Foils

Neutron detectors in the core and thermal column were indium foils of reported purity 99.97%. The foils were 1 cm. square and 0.002 in. thick (35.0 mg./cm.^{2}); each foil was weighed to an accuracy of 0.1 mg., the average weight being 0.0354 g. The gold foils used to calibrate the activity of the indium were circular, .5 in. diameter, and 0.001 in. thick. They were weighed to an accuracy of 0.1 mg., the average weight being 0.0639 g. The indium foils were wrapped in aluminum foil (0.0017 cm. thick) to protect them during irradiation in the reactor; however, no protective cover was required for the gold foils.

Radiation Detection Equipment

A Nuclear-Chicago 2π gas flow detector, Model D-47, equipped with a micromil window was used to detect the β radiation from the activated foils. The detector and foil were enclosed in a lead shield to reduce the background counting rate. The output pulse of the detector was amplified through a Nuclear-Chicago Model D47P preamplifier and was registered on a Nuclear-Chicago decade scaler, Model 186-P.

This particular combination of detector, preamplifier, and decade scaler had been previously calibrated with gold foils activated in a known thermal neutron flux. Operating conditions of the radiation detection equipment were:

(a) Preamplifier gain -- 5

(b) Decade scaler

High voltage -- 2100 volts

Input sensitivity -- 2.5 millivolts

(c) Gas flow detector

gas pressure -- 5 psig.

Standard Radiation Source

A uranium standard source was used to detect small variations in the response of the detection equipment between successive days' observations. The source was marked so that the physical geometry of the source within the lead shield could be kept constant.

EXPERIMENTAL PROCEDURE

General

Neutron activation of indium foil was selected as the method for obtaining the relative flux distribution in the core. The cadmium ratio obtained at selected stations permitted the calculation of the indium saturated thermal activity. This activity was expressed in terms of thermal neutron flux by comparison with the activity of a gold foil used to determine the thermal neutron flux in the thermal column. More detailed discussion of these procedures appears in the subsequent sections.

Selection of Stations in the Reactor

Five basic stations were selected along the vertical length of the fuel plates, the center station falling on the centerline of the fuel within the plates. Two stations were selected near the top and bottom of the plates at a distance of 9 in. from the centerline. These stations were 3 in. inside the outer limits of the fuel inside the cladding. Finally, two intermediate stations were selected at a distance of 4.5 in. from the centerline. The external stringer on the dummy fuel assembly (Figure 2) shows the location of the five vertical stations on one fuel plate.

Figure 2. Dummy fuel assembly

More observations were desired in the south core tank than in the north core tank because of the more stable operating conditions existing in the south tank. Artificial operating conditions were imposed so that the regulating rod was completely withdrawn and remained stationary during the run; consequently, there was no variation of the core geometry in this region. However, the position of the shim-safety rod had to be varied to control the reactor, and this position varied between successive runs, as seen in Table 1. Since this variation in core geometry was unavoidable, fewer observations were desired for the north core tank. An additional requirement was to have more observations in the immediate vicinity of the control rods in order to detect any influence that they may have had on the flux distribution in the core. Lateral stations were selected in accord with these requirements. Figure 1 (a) illustrates the notation for designating these stations, and the stringer inside the dummy fuel assembly (Figure 2) shows a typical location of the foils within the assembly.

Since the data could not be obtained simultaneously for all stations, two additional stations were selected within the thermal column. Station A was a circular depression located 48 in. from the south end of the central stringer in the thermal column. Station B was a similar circular depression located 50 in. from the south end of the stringer 8 in.

Table 1. Reactor operating conditions

Run no.	IBM run no.	Date 1962	Moderator temp., °F In	Moderator temp., °F Out	Reg. rod position in.	Shim rod position in.	Scram time	Reactor power watts
1	320	1-16	88	81	5.5	6.2	1112	0.5
2	321	1-16	89	82	5.8	6.7	1620	0.5
3	327	1-22	88	82	0.0	7.4	1619	0.1
4	333	1-29	89	82	out	4.6	1612	0.1
5	333	1-29	87	81	out	4.4	1700	0.1
6	335	1-31	88	83	out	5.9	0929	0.1
7	338	2-2	87	81	out	4.5	0931	0.1
8	340	2-5	88	82	out	4.7	0942	0.1
9	341	2-5	89	83	out	4.8	1627	0.1
10	342	2-6	88	83	out	5.0	1108	0.1
11	344	2-7	90	83	out	4.9	1024	0.1
12	344	2-7	87	83	out	4.8	1129	0.1
13	347	2-9	84	78	out	4.4	1137	0.1
14	348	2-12	86	80	out	4.8	0950	0.1
15	359	3-15	93	81	out	4.7	1100	0.1
16	361	3-19	86	86	out	4.0	1611	0.1
17	361	3-19	83	83	out	3.4	1706	0.1
18	362	3-21	87	86	out	4.0	1058	0.1
19	362	3-21	86	86	out	4.0	1153	0.1
20	365	3-23	86	85	out	6.2	1043	0.1
21	367	3-28	88	88	out	4.0	1110	20
22	367	3-28	88	87	out	4.0	1152	20
23	369	3-29	87	87	out	6.0	1004	0.1
24	369	3-29	86	85	out	3.8	1051	0.1
25	370	3-30	86	86	out	4.0	1024	0.1
26	372	4-2	87	87	out	4.0	1056	1.0

immediately below the central stringer in the thermal column. Figure 1 (b) shows the positions of these stringers in the thermal column. Foils were irradiated in these standard stations in each run to permit the data of successive runs to be corrected to one common basis.

Foil Irradiation in the Core

The prepared indium foils were taped to rigid Plexiglass stringers, 3/16 in. x 5/8 in. x 36 in., and suspended in the core between the fuel plates. No more than six foils were placed in the core at any one time; the minimum separation of any two of the foils was, in one case, 3.3 in. but in excess of 9 in. in all other cases. To maintain a constant reactor geometry near the south core tank, the regulating rod was completely withdrawn for each run, and the reactor was controlled manually with the shim-safety rod. The reactor operator attempted to maintain a reactor period of 30 sec. while bringing the reactor up to a power of 0.1 watt. After reaching this power level, the reactor was continued in operation for 15 min. before being shut down by a scram. In addition to following the starting procedure described and timing the period of irradiation, the activity of the foils in the thermal column gave a measure of the integrated flux received by the foils in the core.

To obtain cadmium ratios in the core, the foils were enclosed in sheet cadmium 0.010 in. thick, taped to the Plexiglass stringers, and irradiated under the same conditions as the bare foils.

Observation of Foil Activity

The activated foils were removed from the stringers and stripped of the protective aluminum cover. The foils were placed on an aluminum support plate in the lower shelf of the lead chamber, and care was taken to place each foil in the same geometrical position within the chamber. The β decay was observed for a sufficient period of time to attain a statistical accuracy of 1% or better. Most of the foils were sufficiently active so that only a two-minute observation was required. The total events recorded on the decade scaler and the times of beginning and ending the observation were recorded. The standard source was observed both before and after the activity of the foils was measured to ensure that there was no malfunctioning equipment.

Calibration of Indium Foil Activity

Both bare and cadmium-covered indium foils were activated at Station A in the thermal column. The gold foils were

irradiated for 20 minutes at a reactor power of 20 watts in order to ensure that there was sufficient activation for accurate observation of the β decay. The bare indium foil was irradiated for 15 minutes at a reactor power of 0.1 watt; however, the cadmium-covered indium foil was irradiated for 15 minutes at a reactor power of 1.0 watt to attain a greater level of activation than would be possible at a reactor power of 0.1 watt.

RESULTS AND DISCUSSION

The activity of each indium foil irradiated in the thermal column at Stations A and B was calculated. The observed activity was corrected for background, radioactive decay from the time of reactor scram, individual foil weight, and variation in response of the radiation detection equipment. The equation accounting for these factors is

$$A = [r_{obs} - r_b] \frac{e^{\lambda \bar{t}}}{w} \frac{S_{cr}}{S'_{cr}} \text{ cpm./g.} \qquad (1)$$

Appendix A contains the explanation of the term $e^{\lambda \bar{t}}$ in correcting for radioactive decay. The term $\frac{S_{cr}}{S'_{cr}}$ allows for minor variation in the response of the proportional counting equipment or for evaluating the performance of the equipment when one component has been changed. Finally, dividing by the foil weight, W, allows for variation in the individual foil sizes.

The calculation of the specific foil activity involved selecting a common basis to which to adjust the data of the different reactor runs. The activities of the two foils irradiated in Stations A and B for each run were compared with Run 18 in a ratio defined as

$$\text{Ratio}_{i,j} = \frac{A_{18,i}}{A_{i,j}} \qquad (2)$$

where i = run number, and j = A, B.

The selection of Run 18 as a basis for the comparison reflected consideration of a representative waiting time among the observations and a minimum variation between $\text{Ratio}_{i,A}$ and $\text{Ratio}_{i,B}$ for all the runs. The foil activities and the ratios are compiled in Table 2. The percent difference between the Ratios A and B in any one run was arbitrarily defined as

$$\text{Percent difference} = \frac{\text{Ratio}_{i,A} - \text{Ratio}_{i,B}}{\text{Ratio}_{i,A}} 100 \qquad (3)$$

The normalizing factor used to adjust the data to a common basis was the arithmetic average of the ratios:

$$\text{Normalizing factor}_i = \frac{\text{Ratio}_{i,A} + \text{Ratio}_{i,B}}{2} \qquad (4)$$

The specific foil activity of all the foils irradiated in the reactor core was calculated from

$$A_s = A \frac{\text{normalizing factor}}{\text{flux depression factor}} \frac{1}{1 - e^{-\lambda T}} \text{ cpm./g.} \qquad (5)$$

where A was evaluated by Equation 1. The term $1 - e^{-\lambda T}$ corrected the activity to a saturated level. The flux

Table 2. Normalizing factors

Run no.	Foil activity 10^5 cpm./g. A	Foil activity 10^5 cpm./g. B	Ratio with Run 18 A	Ratio with Run 18 B	Percent difference percent of ratio A	Normalizing factor
1	12.17	11.58	0.0865	0.0950	-9.8	0.0907
2	10.97	11.26	0.0936	0.0953	-1.8	0.0945
3	2.092	2.190	0.4909	0.4899	0.2	0.4904
4	2.217	2.411	0.4632	0.4450	3.9	0.4541
5	2.136	2.155	0.4808	0.4979	-3.6	0.4894
6	2.383	2.488	0.4310	0.4313	-0.1	0.4311
7	2.935	3.090	0.3499	0.3472	0.8	0.3486
8	2.264	2.355	0.4536	0.4556	-0.4	0.4546
9	3.320	3.528	0.3093	0.3041	1.7	0.3067
10	2.261	2.359	0.4542	0.4548	0.0	0.4545
11	1.521	1.629	0.6754	0.6588	2.4	0.6671
12	2.178	2.270	0.4715	0.4727	-0.2	0.4721
13	2.285	2.363	0.4494	0.4541	-1.0	0.4518
14	2.308	2.358	0.4450	0.4550	-2.3	0.4500
15	2.228	2.464	0.4610	0.4355	5.5	0.4482
16	2.280	2.250	0.4504	0.4769	-5.9	0.4637
17	2.318	2.256	0.4430	0.4756	-7.4	0.4594
18	1.027	1.073	1.0000	1.0000	0.0	1.0000
19	2.305	2.325	0.4456	0.4615	-3.6	0.4535
20	2.222	2.244	0.4622	0.4782	-3.4	0.4702
23	2.132	2.250	0.4817	0.4769	1.0	0.4793
24	2.313	2.361	0.4440	0.4545	-2.4	0.4492
25	2.279	2.313	0.4506	0.4639	-2.9	0.4573
26	-	24.530	-	0.0437	-	0.0437

depression factor for indium foil in water was that given by Fitch and Drummond (4, p. 16) as 0.910, and the decay constant for indium-116m was 0.01284 min.$^{-1}$ based on a half life of 54.0 min. listed by Strominger et al. (15).

Price (11b, p. 289) discussed the correction necessary to calculate the saturated thermal activity of the cadmium-covered indium foils and gave the two basic relations for F_{Cd} and f_{th} used in these calculations:

$$F_{Cd} = \frac{A_{se}}{A_s(Cd)} \tag{6}$$

$$f_{th} = 1 + \frac{0.34\ \pi r}{\lambda_{tr}} \qquad \text{for } r \ll \lambda_{tr} \tag{7}$$

where

$$\alpha = 1 - e^{-\Sigma_a d}(1 - \Sigma_a d) - \Sigma_a^2 d^2 E_1(-\Sigma_a d) \tag{8}$$

A value of $F_{Cd} = 1.019$ for indium of 35 mg./cm.^{2} thickness was extrapolated from Figure 9-17 (Price, 11b, p. 290); however Equation 7 is not valid for indium foils in water. The radius of a circular foil of one square centimeter area is 0.564 cm., and this dimension is not very much different from λ_{tr} for water, 0.425 cm. Consequently, no correction was made for the flux perturbation, f_{th}, of the cadmium-covered indium foil in water. The calculations then were:

$$A_{st} = \frac{CR - 1}{CR} A_s \qquad (9)$$

where

$$CR = \frac{A_s}{A_s(Cd)\ F_{Cd}} \qquad (10)$$

The specific counting rates of the bare and cadmium-covered foils and the cadmium ratios are compiled in Table 3.

The calibration of indium foil to determine the thermal neutron flux in the reactor core was based on the comparison of saturated thermal activities of gold and indium foils irradiated in the thermal column at Station A. The activities of the gold foils were corrected much the same as previously stated for the indium foils. The specific foil activity was calculated with Equations 1 and 5, in which the flux depression factor was not used and the decay constant was 1.783×10^{-4} min.$^{-1}$ based on a half life of 2.70 days listed by Strominger et al. (15, p. 774). The factor F_{Cd} for cadmium-covered gold foil was 1.01 (Martin, 10, p. 52). Baucom (2) listed the macroscopic absorption cross section of gold as 5.83 cm.$^{-1}$. Σ_a was corrected to obtain the effective cross section at 73°F before determining α from the graph presented in Price (11b, p. 288). The flux perturbation, F_{th}, was calculated using Equation 7. Using the basic relationships described in Price (11b, p. 287)

$$A'_{st} = F_{th} [A_s - F_{Cd} A_s(Cd)] \quad \text{cpm./g.} \tag{11}$$

the gold foil saturated thermal activity, corrected for flux perturbation, was determined. Then the thermal neutron flux at Station A was calculated from the relation

$$\phi_{th} = A'_{st} \frac{S_{cr}}{S'_{cr}} \frac{1}{K} \quad \text{n./cm.}^2\text{-sec.} \tag{12}$$

where K = 2.1284, a calibration constant for the radiation detection equipment to convert the gold foil saturated thermal activity in cpm./g. to units of neutron flux

and S_{cr} = 24,045 cpm., the activity of the standard uranium source at the time of calibration.[1]

The results of the calculations showed that the thermal neutron flux at Station A was 3.890×10^7 n/cm.^{2}-sec. for a reactor power level of 20 watts. It was assumed that the flux at Station A decreased linearly with the reactor power level. With this assumption the thermal flux at 0.1 watt power was 1.945×10^5 n/cm.^{2}-sec.

The calculation of the saturated thermal activity of the indium foils at Station A was identical to that for the gold foils with the exception of the constants which pertain to

---

[1] Danofsky, Richard A., Ames, Iowa. Calibration of the 2π gas flow detector. Private communication. 1962.

Table 3. Reactor core

Station	Specific counting rate for bare foils 10^6 cpm./g.	Specific counting rate for Cd-covered foils 10^6 cpm./g.	Cadmium ratio	Thermal neutron flux 10^6 n/cm.^{2}-sec.
N1(3W)-1	1.80	0.965	1.83	0.290
-3	3.54			
-5	2.40	0.656	3.58	0.602
N1(3E)-2	1.83			
-4	2.24			
N1(7W)-3	4.69			
N2(3W)-1	2.70			
-5	3.51			
N2(5E)-3	4.49			
N2(9E)-3	5.08			
N3(3W)-1	3.03			
-3	5.50			
-5	3.77			
N3(7W)-1	3.63	0.844	4.22	0.965
-3	5.92	1.634	3.56	1.484
-5	3.83	0.915	4.11	1.011
N4(3W)-1	3.24			
-3	5.61			
-5	3.47			
N5(3E)-1	2.96			
-5	3.40			
N5(9W)-1	2.99			
-2	3.09			
-3	4.96			
-4	3.15			
-5	3.15			

Table 3. (Continued)

Station	Specific counting rate for bare foils	Specific counting rate for Cd-covered foils	Cadmium ratio	Thermal neutron flux
	10^6cpm./g.	10^6cpm./g.		10^6n/cm.^{2}-sec.
S6(3W)-1	2.08			
-3	3.17			
S1(3E)-3	4.36			
S1(5E)-3	4.97			
S1(9E)-1	2.65			
-3	4.08			
-5	2.77			
S2(3E)-3	5.83			
S2(5E)-1	3.45			
-3	5.76			
-5	3.55			
S2(9E)-1	3.31			
-3	6.06			
-5	3.56			
S3(3E)-3	5.90			
S3(5E)-1	4.03			
-3	6.96			
-5	4.56			
S3(9E)-1	3.77			
-3	7.07			
-5	3.84			
S4(3W)-1	4.36			
-2	6.65	1.604	4.07	1.747
-3	7.30			
-4	6.47	1.623	3.91	1.679
-5	4.37			

Table 3. (Continued)

Station	Specific counting rate for bare foils	Specific counting rate for Cd-covered foils	Cadmium ratio	Thermal neutron flux
	10^6 cpm./g.	10^6 cpm./g.		10^6 n/cm.^{2}-sec.
54(5W)-1	4.12	1.098	3.68	1.046
-3	7.29			
-5	4.44	1.150	3.79	1.139
54(9W)-1	4.24			
-2	6.35			
-3	7.51	1.853	3.98	1.890
-4	6.70			
-5	4.26			
55(3W)-1	3.68			
-3	5.98			
-5	3.40			
55(5W)-1	4.30	0.865	4.88	1.191
-2	5.23	1.320	3.89	1.353
-3	6.03	1.485	3.99	1.575
-4	5.46	1.352	3.97	1.425
-5	4.61	0.876	5.17	1.297
55(9W)-1	3.48			
-3	7.48			
-5	3.64			
56(3W)-1	2.74			
-3	4.21	1.002	4.22	1.120
56(5W)-1	2.58			
-3	4.21			
-5	2.84			
56(9W)-1	2.64			
-2	3.35			
-3	4.06	1.029	3.89	1.057
-4	3.81			
-5	2.80			

the type of foil being used. It was assumed that the effect of a square foil detector on the flux perturbation would be the same as that of a circular foil of the same area. The radius of an equivalent circular indium foil was then 0.564 cm. Baucom (2, p. 199) listed the macroscopic absorption cross section for In as 7.30 $cm.^{-1}$. This value was corrected to obtain an effective cross section for the absorption of neutrons. Equation 11 was used to determine the saturated thermal activity of the indium foil -- 5.580×10^5 cpm./g. This activity of the foil corresponded to the thermal flux of 1.945×10^5 $n/cm.^2$-sec. at Station A. The thermal neutron flux at stations within the core was then scaled directly from the relationship

$$\phi_{th} = \frac{(\phi_{th})_A}{(A_{sat})_A} A_{st}$$

$$= 0.3486\ A_{st} \quad \text{thermal } n/cm.^2\text{-sec.} \qquad (13)$$

The results of the calculations for the thermal neutron flux appear in Table 3; however, these data are inconclusive to the extent that no correction was made for the flux perturbation of cadmium-covered indium foils in water. Operational commitments of the UTR-10 reactor prevented a more thorough survey of the cadmium ratios in the core. Hence, a comprehensive view of the thermal neutron flux

Table 4. Duplicated data for specific foil activity

Station	Specific foil activity		Difference between A and B	Percent difference between A and B percent of A
	A	B		
	10^6 cpm./g.		10^6 cpm./g.	
N1(3W)-3	3.54	4.16	-0.62	-17.5
N3(7W)-1	3.63	3.46	0.17	4.6
-5	3.83	4.09	-0.26	- 6.8
N5(9W)-3	4.96	4.97	-0.01	- 0.1
S4(5W)-3	7.29	7.64	-0.35	- 4.9
S4(9W)-1	4.24	4.12	0.12	2.8
-5	4.26	4.14	0.12	2.8
S6(5W)-3	4.21	4.24	-0.03	- 0.8

distribution in the core was not obtained.

Two reactor runs which duplicated two previous runs were made to investigate the degree to which the data could be reproduced. Table 4 shows the stations and a comparison of the specific foil activity of the original run in Column A with that of the duplicate run in Column B. In the south core tank, Run 24 was the duplicate of Run 11. The percent difference between these two runs varied more widely than expected on the basis of the statistical counting accuracy. The data obtained in the north tank vary even more. The

marked variation here is attributed to the difference in operating conditions of the reactor. Run 25 attempts to duplicate the results of Run 5, but the proximity of the shim-safety rod and the difference in its position in the two runs, Table 1, have undoubtedly created the large disparity. It is noteworthy that there is a larger difference in shim-safety rod positions for Runs 11 and 24 in the south core tank, but the effect on the activities there was not appreciable because of the 24 in. distance separating the control rod from the nearest point of the tank and the generation of neutrons in the north core tank.

The accuracy of the results compiled in Table 3 was primarily influenced by the manner of selecting a normalizing factor, the accuracy of some of the constants used in the calculations, reactor operator technique in conducting the run, and the omission of a factor for the flux perturbation of cadmium-covered indium foils in water. Of these items, the normalizing factor presents the greatest error. Next in order of magnitude is the omission of F_{th} for the calculation of the thermal neutron flux in the core. Although the literature contains relatively abundant material about flux depression of neutron detectors in a graphite moderator, very little discussion involving a water moderator was found. Reactor operator technique in starting the reactor and maintaining a fixed power manually and the accuracy of the constants

involved in the calculations were the least sources of error. The observed data, the normalizing factors, and the associated standard deviations are presented in Appendix B.

All the calculations were carried to five significant figures, although some of the constants were given only to three significant figures; the tabulated results are rounded to four significant figures in Table 2, which contains the intermediate data used in subsequent calculations. In Table 3 the final results of the calculations are correct to three significant figures.

The specific foil activities in Table 3 have been plotted in a series of graphs to illustrate the neutron flux distribution in the reactor core. Figure 3 shows how the flux in the south core tank changes in the direction of the X and Y axes in a plane of constant Z value. Comparison of the three parts shows that the neutron flux lacks symmetry with respect to the vertical centerline of the core tank. This effect is more clearly demonstrated by the curves for Y Station 3 at the horizontal centerline of the fuel assembly than for Stations 1 and 5 at the top and bottom of the fuel assembly. From the outer edge of the tank toward the centerline, the flux increases more rapidly in the west half of the tank than occurs in the east half. Although the maximum points of the curves are not well defined by observed data, the relative magnitudes of the flux in fuel assemblies S3 and S4 indicate

that the maximum lies within S4, rather than on the vertical centerline between S3 and S4. The anti-symmetrical distribution of the flux with respect to this centerline is attributed to the influence of the safety rod. The size of the regulating rod is 2 in. x 2 in. x 1/8 in., whereas the size of the safety rod is 7 in. x 8 in. x 1/8 in. (1). The greater amount of Boral in the safety rod depresses the flux on the east side of the tank at fuel assemblies S4, S5, and S6. This effect is evident to a much less degree at the top of the core tank at 2 Stations 5W and 9W. In Figure 3 (b) the difference in the magnitude of the flux at the top and bottom of the fuel assembly is more marked than is evident in Figure 3 (a and c) and indicates lack of a symmetrical distribution about the horizontal centerline of the fuel assembly.

There are three data points shown in Figure 3 that are considered in error -- two in Part b and one in Part c. These three points were obtained during Run 13, but the additional three points obtained in the same run appeared to give satisfactory results. When all the foils for the run had been observed and the proportional counter was checked with the standard source, a low counting rate for the standard was noted. Examination of the equipment revealed that the regulated gas pressure had fallen from 5 psig. to 3.95 psig. and thereby made the reliability of the data questionable. Since

the foils from Stations A and B were the last foils of the run to be observed, the normalizing factor was greater than it should have been. Consequently, the specific foil activities were too high for part of the data and apparently consistent for the remaining data of Run 13.

Figure 4 shows the flux magnitude in the south core tank in the direction of the Z and Y axes in a plane of constant X value. Since only the three data points were obtained, the shape of the curve is inconclusive, and only the relative magnitudes of the flux are intended to be shown. Figure 5 shows the same type of information for 7 stations in the east half of the fuel assembly; however, these points were obtained from the curves of Figure 3 and do not represent observed data. The inconsistency of the data obtained in Run 13 is again evident in Figure 4.

Purely by circumstance, the stations chosen in the fuel assemblies at S6(5W) and S1(5E) were immediately adjacent to dummy fuel plates in the assembly.[1] Unfortunately the data are not sufficient to determine the influence of the absence of fuel in this region; however, Figure 3 and Figure 4 show no marked change in the flux as a result of the dummy fuel plates.

---

[1]Murphy, Glenn, Ames, Iowa. Fuel inventory of the UTR-10 reactor. Private communication. 1962.

Figure 6 shows the change in the flux in the direction of the Y and Z axes at a constant value of X. Although the magnitudes of the flux are much the same, there is yet indication of the lack of symmetry with respect to the horizontal axis through the tank. The fuel assemblies S4 and S6 exhibit noticeable anti-symmetry, but the data for S5 are inconclusive as a result of the faulty data of Run 13.

Figure 7 shows the flux distribution in the north and south core tanks at 7 stations adjacent to the control rods and provides a comparison of the flux magnitude in the two tanks. At the top of fuel assemblies N1, N2, and N3 the flux is greatly depressed in relationship to the flux at the bottom of the assembly, and the contrast with the conditions in the comparable fuel assemblies in the south core tank is marked. This effect is attributed to the proximity of the shim-safety rod and its action as a neutron sink. Because of the varying position of the shim-safety rod in successive runs, the shape of the curves drawn for the north core tank is somewhat questionable, but the relative magnitudes should be representative of the actual conditions in the tank. Table 5 assists in comparing the flux magnitude in the two tanks. The specific foil activities in comparable stations near the control rods are listed vertically to provide a ready reference. At all stations in the north core tank the flux is significantly lower than that of the south core tank, and

Table 5. Specific foil activity

Fuel assembly	Irradiation activity 10^6 cpm./g.				
	1	2	3	4	5
N1(3W)	1.797		3.536		2.396
S6(9W)	2.643	3.353	4.081	3.814	2.797
N2(3W)	2.701				3.514
S5(9W)	3.481		7.475		3.645
N3(3W)	3.032		5.495		3.774
S4(9W)	4.238	6.346	7.511	6.701	4.262
N4(3W)	3.238		5.609		3.472
S3(9E)	3.770		7.074		3.844
N5(3E)	2.964				3.405
S2(9E)	3.307		6.055		3.561
N6(3W)	2.078		3.166		
S1(9E)	2.650		4.084		2.774

the greatest contrast is shown between the flux levels along the horizontal centerline of the core tanks. The data do not permit determining whether the flux depression is caused solely by the presence of the shim-safety rod or if, in addition to the control rod, other factors are acting to depress the flux.

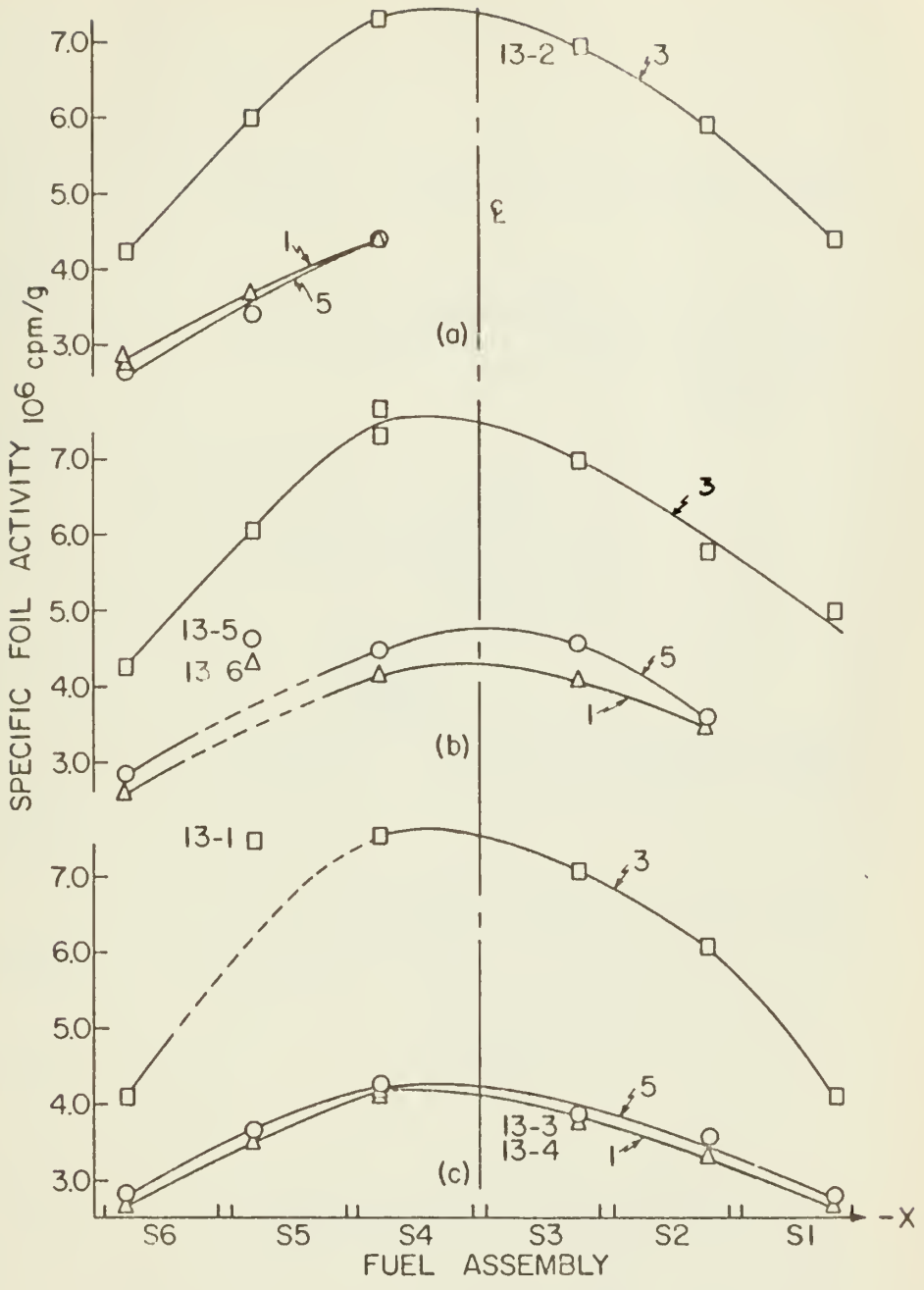

Figure 3. Neutron flux distribution in the south core tank
(a) Z stations, 3 east and 3 west
(b) Z stations, 5 east and 5 west
(c) Z stations, 9 east and 9 west

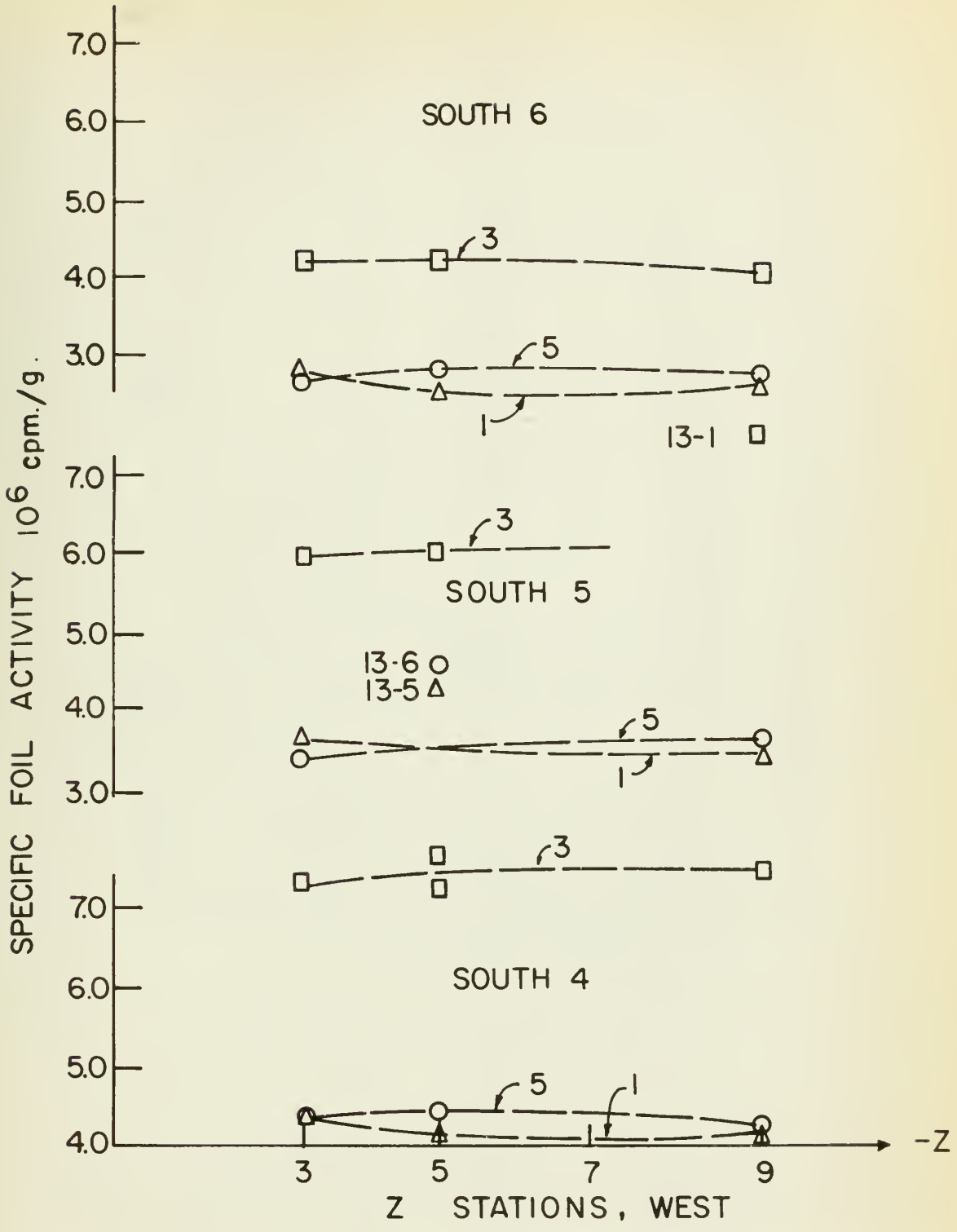

Figure 4. Neutron flux distribution in the south core tank

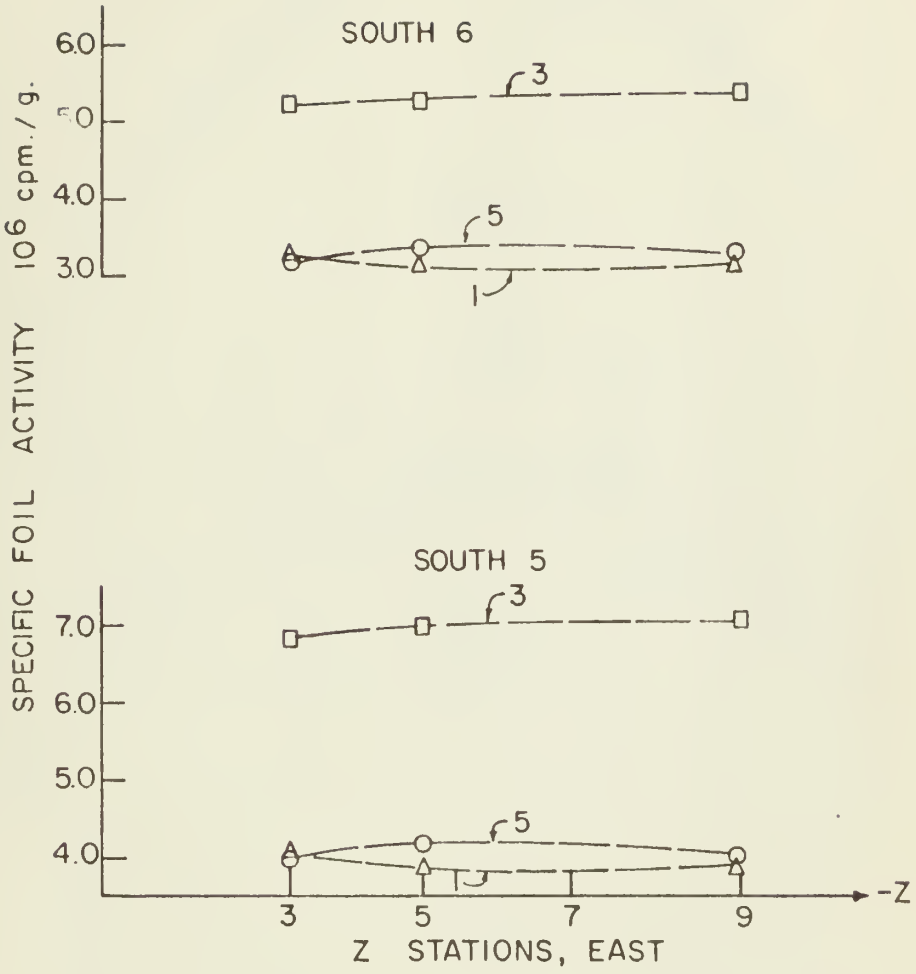

Figure 5. Neutron flux distribution in the south core tank

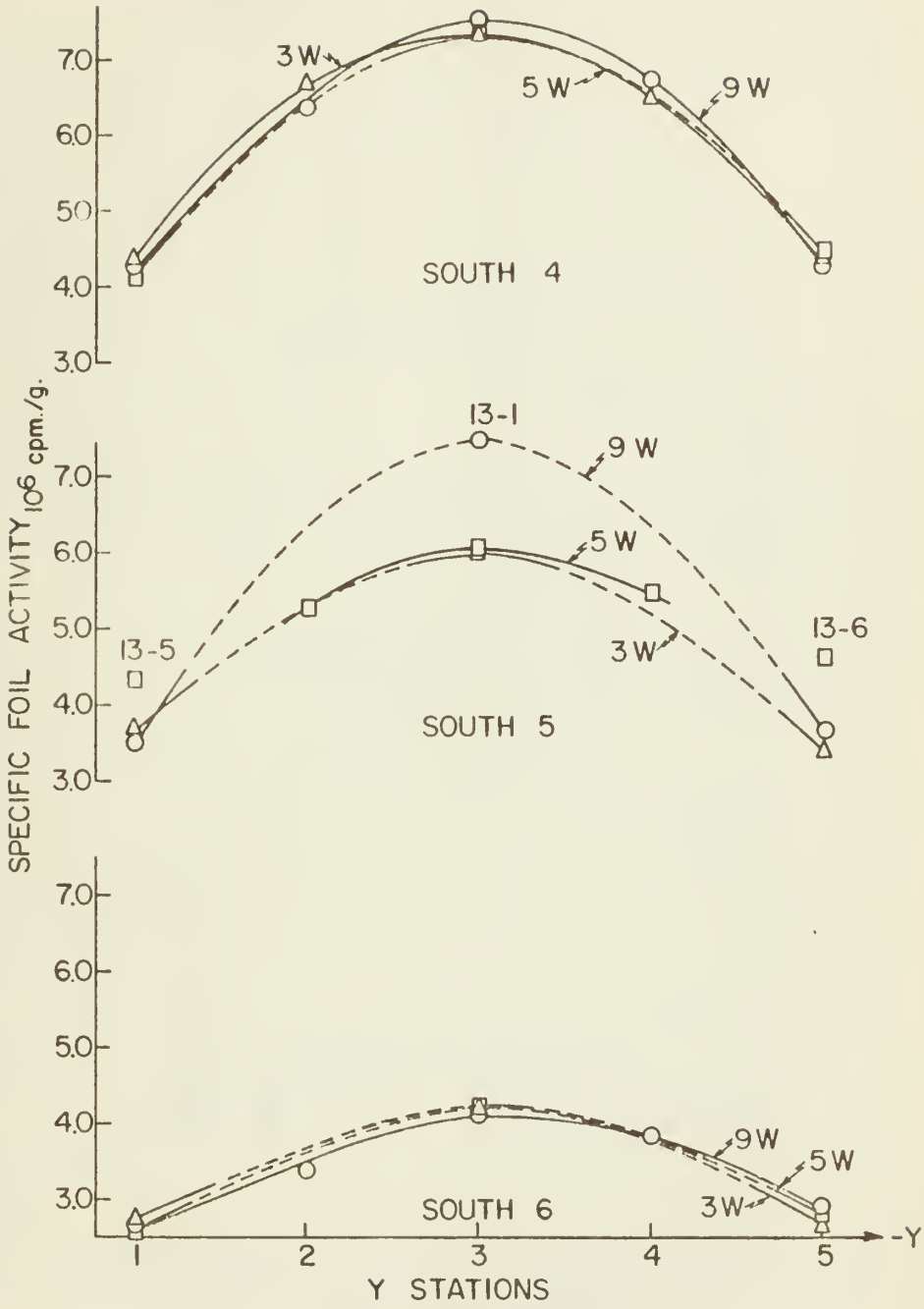

Figure 6. Neutron flux distribution in the south core tank

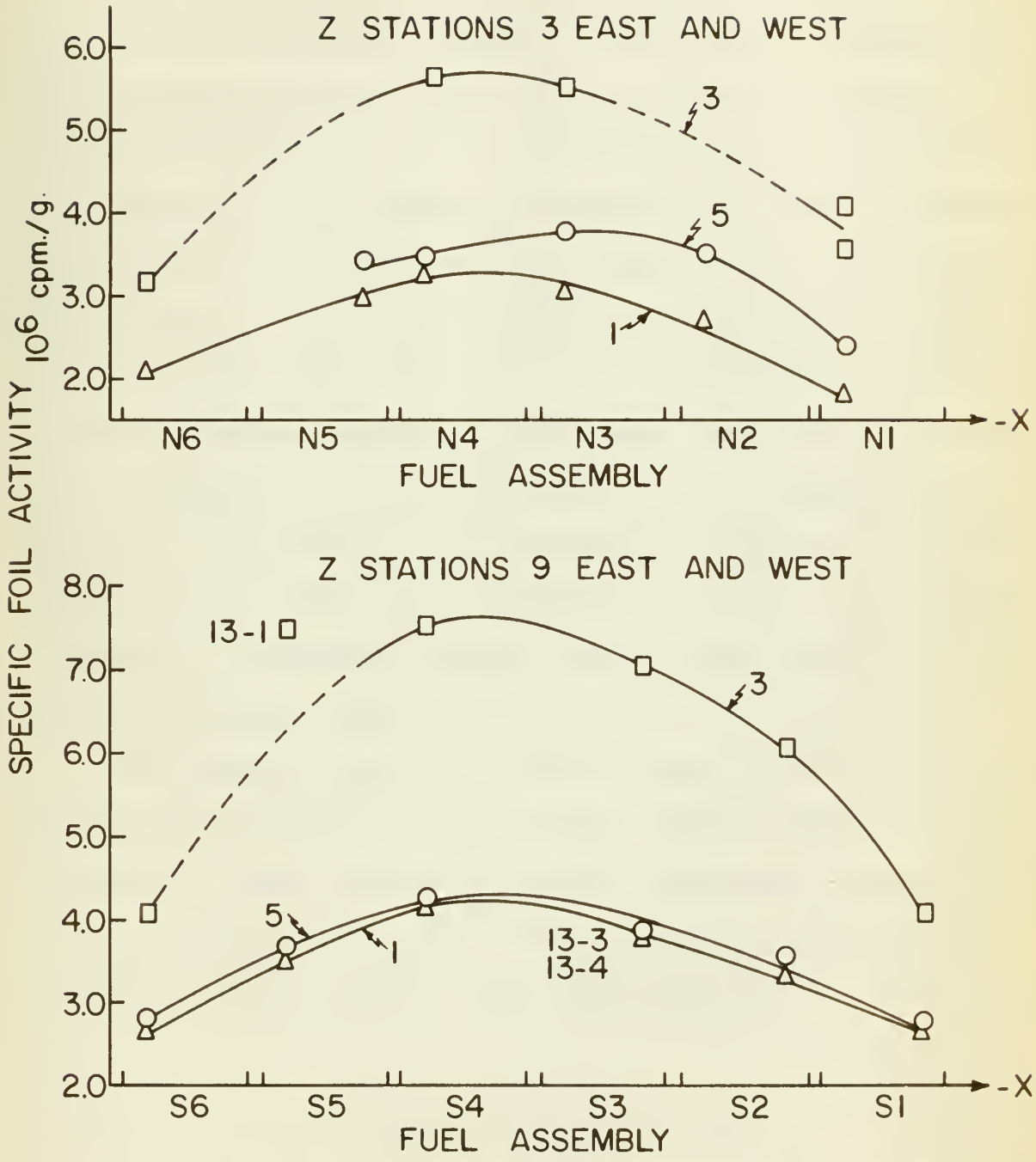

Figure 7. Flux distribution at 7 stations adjacent to the control rods

CONCLUSIONS

The investigation of the neutron flux distribution in the core of the UTR-10 reactor at Iowa State University has been conducted using indium foils as a neutron detector. The restrictions placed on the reactor control rods were that the regulating rod was completely withdrawn and that the reactor power of 0.1 watt was controlled manually with the shim-safety rod. From a study of the activation of the foils in the core, it was evident that the neutron flux distribution in the south core tank was not symmetric with respect to either the vertical or horizontal centerlines of the tank. Comparing the specific foil activities in comparable stations of the north and south core tanks, it was apparent that the flux distribution was not symmetric between the two tanks, the flux in the north tank being depressed below that in the south tank.

The limited survey of cadmium ratios in the core was not sufficient to permit a study of the thermal neutron flux distribution. Among those stations for which the thermal neutron flux was obtained, however, the maximum flux occurred at Station S4(9%)-3 and was 1.89×10^{6} n/cm.^{2}-sec.

SUGGESTIONS FOR FURTHER STUDY

Since the scope of this project was limited by the time available to accumulate data, further investigation might be conducted to obtain a cadmium ratio survey in the south core tank and to determine the thermal neutron flux there. The comparison of the thermal flux distribution with the flux distribution obtained by specific foil activities could be the basis for an extension of the present project.

An alternative proposal might be to examine the effect of the regulating rod position on the thermal neutron flux distribution in the immediate region of the regulating rod. The investigation could be confined to the three fuel assemblies adjacent to the regulating rod and would permit time for a more thorough inquiry into the effects of the regulating rod position on the thermal flux.

A related project might be to investigate the performance of the 2" gas flow detector when the gas flow rate is varied from the designed rate. The uranium standard source could be used to provide a constant level of radiation while the gas pressure to the metering orifice was varied. The response of the detector under varying rates of gas flow then could be examined.

LITERATURE CITED

1. Advanced Technology Laboratories. Division of American-Standard. Installation and maintenance manual; control rods for UTR-10 reactor. Mountain View, Calif., Author. 1959.

2. Baucom, H. H., Jr. Nuclear data for reactor studies. Nucleonics 18, No. 11: 198-200. Nov. 1960.

3. Bothe, W. Zur Methodik der Neutronensonden. Zeitschrift für Physik 120: 437-449. 1943.

4. Fitch, S. H. and Drummond, J. E. Neutron detector perturbations. U. S. Atomic Energy Commission Report LRL-95. [California Research and Development Co. Livermore Research Lab., Livermore, Calif.] 1954.

5. Greenfield, Moses A., Koontz, Roscoe L., and Jarrett, Alan A. Absolute thermal neutron determination. I. Measuring the ratio of thermal to resonance neutron densities using thick indium foils. U. S. Atomic Energy Commission Report NAA-SR-1137. [North American Aviation, Inc., Downey, Calif.] 1955.

6. _____, _____, and _____. Absolute thermal neutron determination. III. Absolute thermal neutron flux. U. S. Atomic Energy Commission Report NAA-SR-1137. [North American Aviation, Inc., Downey, Calif.] 1957.

7. Klema, E. D. and Ritchie, R. H. Thermal neutron flux measurements in graphite using gold and indium foils. Physical Review 87: 167. 1952.

8. Koontz, Roscoe L., Greenfield, Moses A., and Jarrett, Alan A. Absolute thermal neutron determination. II. Absolute beta counting of indium foils. U. S. Atomic Energy Commission Report NAA-SR-1137. [North American Aviation, Inc., Downey, Calif.] 1955.

9. Kunstadter, John W. A correction to be applied to the activity of neutron-activated cadmium-covered indium foils. Physical Review 78: 484. 1950.

10. Martin, D. H. Correction factors for Cd-covered-foil measurements. Nucleonics 13, No. 3: 52-53. Mar. 1955.

11a. Overman, Ralph T. and Clark, Herbert M. Radioisotope techniques. New York, N. Y., McGraw-Hill Book Co., Inc. 1960.

11b. Price, William J. Nuclear radiation detection. New York, N. Y., McGraw-Hill Book Co., Inc. 1958.

12. Ritchie, R. H. and Eldridge, H. B. Thermal neutron flux depression by absorbing foils. Nuclear Science and Engineering 8: 300-311. 1960.

13. Skyrme, T. H. R. Reduction in neutron density caused by an absorbing disc. 2nd ed. United Kingdom Atomic Energy Authority Report MS-91. 1961.

14. Sola, Alain. Flux perturbation by detector foils. Nucleonics 18, No. 3: 78-81, 141. Mar. 1960.

15. Strominger, D., Hollander, J. M., and Seaborg, G. T. Table of isotopes. Reviews of Modern Physics 30: 585-904. 1958.

16. Thompson, M. W. Some effects of the self-absorption of neutrons in neutron-detecting foils. Journal of Nuclear Energy 2: 286-290. 1956.

17. Tittle, C. W. Slow-neutron detection by foils. I. Nucleonics 8, No. 6: 5-9. Jun. 1951; II. Nucleonics 9, No. 1: 60-67. Jul. 1951.

ACKNOWLEDGMENTS

The author wishes to express a sincere gratitude to his major professor, Dr. Glenn Murphy, for his interest and guidance throughout the course of study at Iowa State University. Thanks are due, in particular, to Mr. Richard A. Danofsky for his original suggestion and continued active interest in the project and to Mrs. Virginia P. Denisen for her assistance during the experimental portion of the investigation.

This thesis concludes three years of postgraduate education sponsored by the United States Navy. I wish to express my appreciation to the United States Naval Postgraduate School and to the United States Navy for the two years' study in Aeronautical Engineering at Monterey, California, and for the additional year of study in Nuclear Engineering at Iowa State University.

APPENDIX A: CORRECTION OF OBSERVED ACTIVITY FOR WAITING TIME

The activated foils were observed at some time t_1 after reactor shutdown, and the observation period ended at a time t_2. The total of observed events, N, occurred in the time interval $t_2 - t_1$. Defining $\Delta = t_2 - t_1$, the average observed decay rate, $\bar{R}$, is then

$$\bar{R} = \frac{N}{\Delta} \tag{14}$$

The question then arises as to what time in the observation period was this average decay rate applicable.

Let R_o = the initial decay rate at reactor shutdown, cpm.

δ = the elapsed time after t_1 at which $\bar{R}$ is applicable, min.

$\bar{t}$ = the time at which $\bar{R}$ is applicable, min.

The decay rate at any time t after reactor shutdown is

$$R(t) = R_o\, e^{-\lambda t} \tag{15}$$

and the total observed events in the time interval Δ are

$$N = \int_{t_1}^{t_2} R_o \, e^{-\lambda t} \, dt$$

$$= -\frac{1}{\lambda} R_o \left(e^{-\lambda t_2} - e^{-\lambda t_1} \right) \tag{16}$$

Equation 14 then becomes

$$\bar{R} = \frac{-R_o \left(e^{-\lambda t_2} - e^{-\lambda t_1} \right)}{\lambda \Delta} \tag{17}$$

The average observed decay rate is then defined as

$$\bar{R} = R_o \, e^{-\lambda \bar{t}} \tag{18}$$

Combining Equations 17 and 18 and simplifying the expression,

$$-\lambda \bar{t} = \ln \left[-\frac{1}{\lambda \Delta} \left(e^{-\lambda t_2} - e^{-\lambda t_1} \right) \right]$$

$$\bar{t} = -\frac{1}{\lambda} \ln \left[e^{-\lambda t_1} \left(-\frac{1}{\lambda \Delta} \right) \left(e^{-\lambda \Delta} - 1 \right) \right]$$

$$= t_1 - \frac{1}{\lambda} \ln \left[\frac{1}{\lambda \Delta} \left(1 - e^{-\lambda \Delta} \right) \right] \tag{19}$$

Since $\bar{t} = t_1 + b$,

$$b = -\frac{1}{\lambda} \ln \left[\frac{1 - e^{-\lambda \Delta}}{\lambda \Delta} \right] \tag{20}$$

Expanding the exponential term of Equation 20 in an infinite series,

$$e^{-\lambda\Delta} = 1 - \lambda\Delta + \frac{(\lambda\Delta)^2}{2!} - \frac{(\lambda\Delta)^3}{3!} + \frac{(\lambda\Delta)^4}{4!} - \ldots \quad (21)$$

$$\frac{1 - e^{-\lambda\Delta}}{\lambda\Delta} = 1 - \frac{(\lambda\Delta)}{2!} + \frac{(\lambda\Delta)^2}{3!} - \frac{(\lambda\Delta)^3}{4!} + \ldots \quad (22)$$

The infinite series expansion for ln (1 + x) is

$$\ln (1 + x) = x - \frac{x^2}{2} + \frac{x^3}{3} - \frac{x^4}{4} + \ldots \quad (23)$$

Retaining all the terms of Equation 22 through the cubic term

$$\ln \left[\frac{1 - e^{-\lambda\Delta}}{\lambda\Delta}\right] \cong \ln \left\{1 - \left[\frac{\lambda\Delta}{2!} - \frac{(\lambda\Delta)^2}{3!} + \frac{(\lambda\Delta)^3}{4!}\right]\right\} \quad (24)$$

Expanding Equation 24 in the series approximation of Equation 23, retaining all terms through the cubic term, and substituting in Equation 20,

$$\delta \cong \frac{\Delta}{2} - \frac{\lambda\Delta^2}{24} \text{ min.} \quad (25)$$

Equation 25 retains all the cubic terms in the two series expansions and is valid where $\lambda\Delta$ is a small quantity in comparison to one.

The decay constant for In^{116m} is 0.012836 min.$^{-1}$ and

substituting this value in Equation 25,

$$\lambda \cong \frac{\Delta}{2} - \Delta^2 \, (0.0005348) \quad \text{min.} \tag{26}$$

Since the time interval, Δ, was less than ten minutes in all observations of the indium foil, the observed decay rate is assumed to be applicable at the midpoint of the observation period; the error involved is less than 3.3 seconds for a ten minute observation.

The decay constant for Au^{198} is 1.7828×10^{-4} min.$^{-1}$, and, substituting this value in Equation 25,

$$\lambda \cong \frac{\Delta}{2} - 7.428 \times 10^{-6} \, \Delta^2 \quad \text{min.} \tag{27}$$

Again, the time interval of observation was so short that the midpoint of the period was considered as the time when the observed decay rate was applicable. For an eleven minute observation, the error involved is less than 0.06 second.

Since most of the observation periods for both the indium and gold foils were two minutes, the second term of Equation 25 may be neglected. Consequently, the foil activity at the time of observation was corrected for the elapsed time between reactor shutdown and the middle of the counting period. As shown in Equation 18

$$P_o = \overline{R} \, e^{\lambda \overline{t}} \qquad \text{where } \overline{t} = t_1 + \frac{\Delta}{2} \tag{28}$$

APPENDIX B: STATISTICAL ACCURACY OF DATA

The mathematical relationships pertaining to a Poisson distribution (as cited in Overman and Clark, 11a, p. 114) have been applied to the observed data to obtain an indication of the accuracy attained in the measurement of the foil activity. Since, in most cases, there was only one observation for each foil, the standard deviation of the decay rate was obtained from the relation

$$\sigma_R = \left(\frac{h}{t}\right)^{1/2} \tag{29}$$

For the difference of two quantities, X and Y, each having an associated error σ_X and σ_Y, respectively, the standard deviation was calculated with the expression

$$\sigma_D = (\sigma_X^2 + \sigma_Y^2)^{1/2} \tag{30}$$

To obtain the standard deviation of the product of two independent quantities, X and Y, the relationship used in the calculations was

$$\sigma_P = (X\ Y)\left(\frac{\sigma_X^2}{X^2} + \frac{\sigma_Y^2}{Y^2}\right)^{1/2} \tag{31}$$

The standard deviation of the quotient of two independent

quantities, X and Y, was calculated from the relationship

$$\sigma_Q = \left(\frac{X}{Y}\right)\left(\frac{\sigma_X^2}{X^2} + \frac{\sigma_Y^2}{Y^2}\right)^{1/2} \qquad (32)$$

These four basic equations were used to calculate the standard deviations of the observed data and of the normalizing factors derived from these data. The results of these calculations are shown in Table 6. The background rate was rounded to the nearest integral number before it was subtracted from the observed decay rate; however, decimal fractions of the decay rates were retained in the standard deviation to show the effect of combining the rates.

Table 6. Statistical accuracy of the observed data and normalizing factors

Run no.	Station	Observed decay rate cpm.	Background cpm.	Net decay rate cpm.	Normalizing factor
1	N3(2W)-3	24680 ± 111.1	17.8 ± 1.3	24662 ± 111.1	0.0907 ± 0.0020
	N3(5W)-3	28734 ± 119.9		28716 ± 119.9	
	N3(10W)-3	23268 ± 107.9		23250 ± 107.9	
	N4(3W)-3	30174 ± 122.8		30156 ± 122.8	
	N4(9W)-3	27106 ± 116.4		27088 ± 116.4	
	A	19549 ± 98.9		19531 ± 98.9	
	B	17433 ± 93.4		17415 ± 93.4	
2	N4(3E)-3	6373 ± 56.4	17.8 ± 1.3	6355 ± 56.4	0.0945 ± 0.0023
	N4(9E)-3	38618 ± 139.0		38600 ± 139.0	
	N3(5W)-1	2691 ± 25.9		2673 ± 26.0	
	-3	7982 ± 63.2		7964 ± 63.2	
	-5	2990 ± 27.3		2972 ± 27.4	
	A	4250 ± 37.6		4232 ± 37.7	
	B	4118 ± 37.1		4100 ± 37.1	

Table 6. (Continued)

Run no.	Station	Observed decay rate cpm.	Background cpm.	Net decay rate cpm.	Normalizing factor
3	M4(5E)-3	29359 ± 121.2	17.5 ± 1.1	29341 ± 121.2	0.4904 ± 0.0136
	M2(3E)-3	24113 ± 109.8		24095 ± 109.8	
	M2(3E)-3	29618 ± 121.7		29600 ± 121.7	
	M6(9W)-3	20032 ± 100.1		20014 ± 100.1	
	A	3932 ± 36.2		3914 ± 36.2	
	B	3281 ± 33.1		3263 ± 33.1	
4	M1(3W)-1	5201 ± 51.0	16.5 ± 1.3	5186 ± 51.0	0.4541 ± 0.0111
	-5	6172 ± 55.6		6156 ± 55.6	
	M5(9W)-1	6852 ± 58.5		6836 ± 58.5	
	-5	8688 ± 65.9		8672 ± 65.9	
	A	1319 ± 12.8		1302 ± 12.9	
	B	1364 ± 13.1		1348 ± 13.1	

Table 6. (Continued)

Run no.	Station	Observed decay rate cpm.	Background cpm.	Net decay rate cpm.	Normalizing factor
5	A1(3a)-3	7476 ± 61.1	15.9 ± 1.3	7460 ± 61.1	0.4894 ± 0.0120
	A5(9a)-3	12037 ± 77.5		12021 ± 77.5	
	A3(7a)-1	7540 ± 61.4		7524 ± 61.4	
	-5	7276 ± 60.3		7260 ± 60.3	
	A	2217 ± 21.1		2201 ± 21.1	
	B	2083 ± 20.4		2067 ± 20.4	
6	A1(3a)-1	6042 ± 55.0	15.9 ± 1.3	6026 ± 55.0	0.4311 ± 0.0104
	-5	3907 ± 44.2		3891 ± 44.2	
	A3(7a)-1	5798 ± 53.8		5782 ± 53.8	
	-3	10114 ± 71.1		10098 ± 71.1	
	-5	6078 ± 55.1		6062 ± 55.1	
	A	4340 ± 38.0		4324 ± 38.0	
	B	4278 ± 37.8		4262 ± 37.8	

Table 6. (Continued)

Run no.	Station	Observed decay rate cpm.	Background cpm.	Net decay rate cpm.	Normalizing factor
7	N1(3E)-2	14569 ± 85.4	16.2 ± 1.3	14553 ± 85.4	0.3486 ± 0.0103
	-4	15217 ± 87.2		15201 ± 87.2	
	N5(9W)-2	20396 ± 101.0		20380 ± 101.0	
	-4	25280 ± 112.3		25264 ± 112.3	
	N3(7W)-3	24326 ± 110.3		24310 ± 110.3	
	A	3753 ± 35.4		3737 ± 35.4	
	B	3872 ± 35.9		3856 ± 35.9	
8	N2(3W)-1	15089 ± 86.9	19.0 ± 1.4	15070 ± 86.9	0.4546 ± 0.0111
	-5	20795 ± 102.0		20776 ± 102.0	
	N4(3W)-1	17209 ± 92.8		17190 ± 92.8	
	-5	16452 ± 90.8		16433 ± 90.8	
	N2(9E)-3	25966 ± 113.9		25947 ± 113.9	
	A	3194 ± 28.3		3175 ± 28.3	
	B	2937 ± 27.1		2918 ± 27.1	

Table 6. (Continued)

Run no.	Station	Observed decay rate cpm.	Background cpm.	Net decay rate cpm.	Normalizing factor
9	N3(3W)-1	16786 ± 91.6	19.0 ± 1.4	16767 ± 91.6	0.3067 ± 0.0735
	-5	18289 ± 95.6		18270 ± 95.6	
	N5(3E)-1	13658 ± 82.6		13639 ± 82.6	
	-5	18749 ± 96.9		18730 ± 96.9	
	N1(7W)-3	28501 ± 119.3		28482 ± 119.3	
	A	4146 ± 37.2		4127 ± 37.2	
	B	4302 ± 37.9		4283 ± 37.9	
10	N3(3W)-3	44010 ± 148.3	18.0 ± 1.3	43992 ± 148.3	0.4545 ± 0.0108
	N2(5E)-3	37965 ± 137.8		37947 ± 137.8	
	N4(3W)-3	42384 ± 145.6		42366 ± 145.6	
	N6(3W)-3	21526 ± 103.7		21508 ± 103.7	
	-1	15356 ± 87.6		15338 ± 87.6	
	A	4650 ± 39.4		4632 ± 39.4	
	B	4282 ± 37.8		4264 ± 37.8	

Table 6. (Continued)

Run no.	Station	Observed decay rate cpm.	Background cpm.	Net decay rate cpm.	Normalizing factor
11	36(5W)-3	7403 ± 60.8	17.1 ± 0.9	7386 ± 60.8	0.6671 ± 0.0163
	34(5W)-3	11644 ± 76.3		11627 ± 76.3	
	34(9W)-1	6814 ± 58.4		6797 ± 58.4	
	-5	6399 ± 56.6		6382 ± 56.6	
	36(3W)-1	3801 ± 43.6		3784 ± 43.6	
	A	1316 ± 12.8		1299 ± 12.8	
	B	1444 ± 13.4		1427 ± 13.5	
12	34(9W)-3	17887 ± 94.5	17.1 ± 0.9	17870 ± 94.5	0.4721 ± 0.0114
	36(3W)-3	9722 ± 69.7		9705 ± 69.7	
	34(3W)-1	12195 ± 78.1		12178 ± 78.1	
	-5	10020 ± 70.8		10003 ± 70.8	
	36(9W)-1	5413 ± 52.1		5396 ± 52.1	
	-5	5571 ± 52.8		5554 ± 52.8	
	A	2050 ± 20.2		2033 ± 20.3	
	B	1884 ± 17.7		1867 ± 17.8	

Table 6. (Continued)

Run no.	Station	Observed decay rate cpm.	Background cpm.	Net decay rate cpm.	Normalizing factor
13	S5(9W)-3	21912 ± 104.7	18.4 ± 1.4	21894 ± 104.7	0.4518 ± 0.0110
	S3(3E)-3	17710 ± 94.1		17692 ± 94.1	
	S3(9E)-1	9288 ± 68.2		9270 ± 68.2	
	-5	11088 ± 75.1		11070 ± 75.1	
	S5(5W)-1	10019 ± 70.8		10001 ± 70.8	
	-5	9504 ± 68.9		9486 ± 68.9	
	A	2216 ± 21.0		2198 ± 21.1	
	B	2165 ± 20.8		2147 ± 20.9	
14	S3(5E)-1	27569 ± 117.4	18.0 ± 1.3	27551 ± 117.4	0.4500 ± 0.0110
	-5	27990 ± 118.3		27972 ± 118.3	
	S3(9E)-3	42285 ± 145.4		42267 ± 145.4	
	S5(3W)-3	43565 ± 147.6		43557 ± 147.6	
	S5(9W)-1	20872 ± 102.2		20854 ± 102.2	
	-5	18959 ± 97.4		18941 ± 97.4	
	A	4786 ± 39.9		4768 ± 40.0	
	B	4660 ± 39.4		4642 ± 39.4	

Table 6. (Continued)

Run no.	Station	Observed decay rate cpm.	Background cpm.	Net decay rate cpm.	Normalizing factor
15	S6(5W)-1	1760 ± 17.1	17.8 ± 1.3	1742 ± 17.2	0.4489 ± 0.0136
	-5	1749 ± 17.1		1731 ± 17.1	
	S4(3W)-3	4070 ± 36.8		4052 ± 36.8	
	S2(9E)-1	2016 ± 20.1		1998 ± 20.1	
	-5	2102 ± 20.5		2084 ± 20.5	
	S2(3E)-3	2950 ± 27.1		2932 ± 27.2	
	A	428 ± 6.5		410 ± 6.7	
	B	438 ± 6.6		420 ± 6.8	
16	S1(3E)-3	11160 ± 74.7	18.1 ± 1.3	11142 ± 74.7	0.4637 ± 0.0116
	S1(9E)-1	6115 ± 55.3		6097 ± 55.3	
	-5	6156 ± 55.5		6138 ± 55.5	
	S4(5W)-1	11141 ± 74.6		11123 ± 74.6	
	-5	9878 ± 70.3		9860 ± 70.3	
	S6(9W)-3	8128 ± 63.7		8110 ± 63.7	
	A	1942 ± 18.0		1924 ± 18.0	
	B	1826 ± 17.4		1808 ± 17.5	

Table 5. (Continued)

Run no.	Station	Observed decay rate cpm.	Background cpm.	Net decay rate cpm.	Normalizing factor
17	S1(5E)-3	17324 ± 93.1	18.1 ± 1.3	17306 ± 93.1	0.4594 ± 0.0114
	S1(9E)-3	13528 ± 82.2		13510 ± 82.2	
	S4(3W)-2	20191 ± 100.5		20173 ± 100.5	
	-4	17912 ± 94.6		17894 ± 94.6	
	S6(9W)-2	9877 ± 70.3		9859 ± 70.3	
	-4	10378 ± 72.0		10360 ± 72.0	
	A	2484 ± 22.3		2476 ± 22.3	
	B	2567 ± 25.1		2549 ± 25.1	
18	S2(5E)-1	6206 ± 54.8	18.0 ± 1.3	6188 ± 54.8	1.0000 ± 0.0273
	-5	5696 ± 53.4		5678 ± 53.4	
	S2(9E)-3	8856 ± 66.6		8838 ± 66.6	
	S5(5W)-2	8277 ± 64.3		8259 ± 64.3	
	-4	8390 ± 64.8		8372 ± 64.8	
	S3(5E)-3	9486 ± 68.8		9468 ± 68.8	
	A	1162 ± 10.8		1144 ± 10.9	
	B	1134 ± 10.6		1116 ± 10.7	

Table 6. (Continued)

Run no.	Station	Observed decay rate cpm.	Background cpm.	Net decay rate cpm.	Normalizing factor
19	S4(9W)-2	12682 ± 79.6	18.0 ± 1.3	12664 ± 79.6	0.4535 ± 0.0107
	-4	11908 ± 77.2		11890 ± 77.2	
	S5(3W)-1	5642 ± 53.1		5624 ± 53.1	
	-5	6964 ± 58.9		6946 ± 58.9	
	S2(5E)-3	9193 ± 67.8		9175 ± 67.8	
	S5(5W)-3	8598 ± 65.6		8580 ± 65.6	
	A	1644 ± 12.8		1626 ± 12.9	
	B	1577 ± 12.6		1559 ± 12.7	
20	S4(3W)-2	5255 ± 51.3	15.0 ± 1.2	5240 ± 51.3	0.4702 ± 0.0112
	-4	5061 ± 50.3		5046 ± 50.3	
	S5(5W)-1	2489 ± 22.3		2474 ± 22.3	
	-3	3869 ± 35.9		3854 ± 35.9	
	-5	2446 ± 22.1		2431 ± 22.1	
	S6(9W)-3	2630 ± 25.6		2615 ± 25.7	
	A	1436 ± 13.4		1421 ± 13.5	
	B	1537 ± 13.9		1522 ± 13.9	

Table 6. (Continued)

Run no.	Station	Observed decay rate cpm.	Background cpm.	Net decay rate cpm.	Normalizing factor
21	A	18433 ± 96.0	20.2 ± 1.4	18413 ± 96.0	-
	B	20003 ± 100.0		19983 ± 100.0	
22	A	985 ± 9.5	20.2 ± 1.4	965 ± 9.6	-
	B	1305 ± 12.0		1285 ± 12.1	
23	24(5N)-1	5354 ± 51.8	18.1 ± 1.3	5336 ± 51.8	0.4793 ± 0.0116
	-5	5056 ± 50.3		5038 ± 50.3	
	24(9W)-3	7896 ± 62.8		7878 ± 62.8	
	25(5W)-2	6860 ± 58.5		6842 ± 58.5	
	-4	5768 ± 53.7		5750 ± 53.7	
	26(3W)-3	3837 ± 35.8		3819 ± 35.8	
	A	2084 ± 20.4		2066 ± 20.5	
	B	1906 ± 17.8		1888 ± 17.9	

Table 6. (Continued)

Run no.	Station	Observed decay rate cpm.	Background cpm.	Net decay rate cpm.	Normalizing factor
24	S6(5W)-3	17258 ± 92.9	18.1 ± 1.3	17240 ± 92.9	0.4492 ± 0.0109
	S4(5W)-3	28634 ± 120.0		28616 ± 120.0	
	S4(9W)-1	16143 ± 89.8		16125 ± 89.8	
	-5	15399 ± 87.7		15381 ± 87.7	
	S6(3W)-1	9889 ± 70.3		9871 ± 70.3	
	-5	8450 ± 65.0		8432 ± 65.0	
	A	2214 ± 21.0		2196 ± 21.1	
	B	2140 ± 20.7		2122 ± 20.7	
25	N1(3W)-3	20114 ± 100.3	18.7 ± 1.4	20095 ± 100.3	0.4573 ± 0.0109
	N5(9W)-3	25032 ± 111.9		25013 ± 111.9	
	N3(7W)-1	15069 ± 86.8		15050 ± 86.8	
	-5	15858 ± 89.1		15839 ± 89.1	
	A	4201 ± 37.4		4182 ± 37.4	
	B	3975 ± 36.1		3956 ± 36.1	
26	A	3523 ± 34.3	15.3 ± 1.2	3508 ± 34.3	0.0437 ± 0.0006
	B	60488 ± 173.9		60473 ± 173.9	